SHACK-HARTMANN WAVEFRONT SENSOR TESTING OF AERO-OPTIC PHENOMENA*

Daniel R. Neal
WaveFront Sciences, Inc., 15100 Central S.E. Albuquerque, NM 87123
(505) 275-4747, FAX (505)275-4749, drneal@wavefrontsciences.com

Eric Hedlund, Melissa Lederer, Arnold Collier, Charles Spring, Bill Yanta
Naval Surface Warfare Center (K24), 10901 New Hampshire Ave, Silver Spring, MD 20903
(301)394-2095, Collier.Arnold@hap.arnold.af.mil

ABSTRACT

Missile interceptor seeker windows undergo significant heating and stress during supersonic flight. These effects lead to window and flow field distortions that can significantly degrade the image quality on the seeker. We have applied a Shack-Hartmann wavefront sensor for measuring these effects in ground test. The Shack-Hartmann sensor measured the near-field intensity and phase distribution. Because these distributions are linear, relative (or flow on/flow off) measurements can be made where test instrumentation errors can be subtracted out. The image quality, or point spread function, can be computed from these near field measurements. This allows for measurement of the aero-optic quantities that are a simulation of flight conditions, and an accurate prediction of sensor end-to-end performance.

In making point spread function predictions, it is first necessary to establish that the near-field measurements have sufficient accuracy and resolution. To this end a laboratory experiment was constructed that allows direct comparison between measured point spread function and wavefront sensor based predictions. Excellent results were observed with strong, high spatial frequency aberrations.

The wavefront sensor was then applied to make measurements in supersonic flow. Tests have been conducted of simulated seeker windows at Mach 7 and 8 conditions, and time-resolved wavefront sensor measurements have been made in some conditions. While early results have significant facility induced vibration in some conditions. Nevertheless, aero-thermal window heating has been observed in low stress conditions.

Keywords: Aero-optical effects, wavefront sensors, Shack-Hartmann sensors, boresight error, optical seekers, Aerothermal effects, point spread function

1. INTRODUCTION

1.1 Previous test methodologies

A wide variety of different test methodologies have been developed for aero-optical measurements. These include schlieren, two-pulse holography, and interferometry[1,2], along with a host of other methods. Successful measurements have been made in the wind tunnel using these techniques. However, in many cases these experiments were very difficult, and often resulted in a single snapshot measurement during each run. It was extremely difficult to remove vibration effects and get accurate, quantitative measurements. Techniques are needed which have good sensitivity, temporal and spatial resolution, and which are insensitive to vibration. Furthermore, these techniques should be as simple and robust as possible, so that the focus of the measurement effort can be the results, and not the experimental method.

1.2 The Shack-Hartmann wavefront sensor

In the last several years there have been a number of advances in new sensors. CCD technology has greatly improved, resulting in high frame rate cameras with electronic shuttering. These cameras are easily integrated with computer data acquisition. This technology, along with the development of micro-optics technology, has led to the

development of entirely new sensors that can be applied to fluid measurement problems [3,4].

The Shack-Hartmann wavefront sensor was developed initially for adaptive optics, with the Air Force Phillips laboratory, MIT Lincoln Laboratory, Sandia National Laboratories, and numerous universities playing a role. These sensors are robust, reliable, stable, and have large dynamic range and high sensitivity. They have been used extensively for adaptive optics as well as optical metrology and laser beam characterization[13].

The Shack-Hartmann principle is simple and is based on two concepts. Namely, light travels in a straight line in homogeneous media, and the optical wavefront is the surface normal to the direction of propagation. The Shack-Hartmann sensor uses a lenslet array to spatially divide the incoming light among a large number of sub-apertures, and then measures the wavefront slope over each subaperture. The slope information is used to reconstruct the incident wavefront.

The Department of Defense (DoD) and Department of Energy (DOE) have used wavefront sensors for high-bandwidth adaptive-optics applications for many years. The Shack-Hartmann sensor was developed in 1970-71 by Ben Platt and Roland Shack for a military laser program. It has been used by the Air Force, Army, Navy, BMDO, DOE and various astronomical sites for adaptive optics and wavefront aberration measurement applications[5]. The technology of wavefront reconstruction and analysis has been extensively developed, and can be applied to the design of sensors for measurement applications[12].

The Shack-Hartmann sensor combines a compact package with fast measurement and large dynamic range. All of the information is obtained in a single measurement that can be gated for a fraction of a second. It's simple construction means that it is robust, vibration insensitive, extremely accurate and easy to use.

A wavefront sensor system has several key components. These include a lenslet array and CCD camera (or other detector) as shown in Figure 1, a data acquisition system and computer with analysis and control software. Light that is incident on the lenslet array is broken up into a number of individual beams, each of which focuses on the detector at a different location. Since light always propagates normal to its wavefront, the position of the focal spot is a measure of the average wavefront slope over the lenslet sub-aperture. The data are acquired, the centroid of the focal spots computed, and the wavefront reconstructed from the slope measurements using a specialized integration routine.

The sensor spatial resolution is determined by the lenslet size and spacing. The sensitivity is determined by the

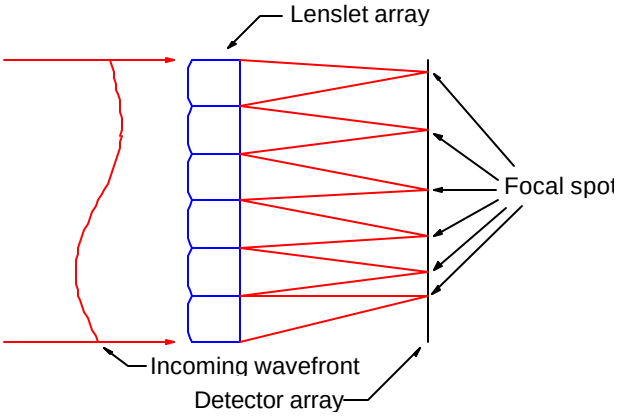

Figure 1 – The basic components of a Shack-Hartmann wavefront sensor.

minimum detectable change in focal spot position (based primarily on detector noise and geometry). Dynamic range is limited by spot overlap.

Advances in micro-optics technology[6] are the key ingredients for wavefront sensor development. Micro-optics technology is the application of integrated circuit manufacturing techniques to the fabrication of optics. The optics are designed on a computer CAD program, then photolithography is used to transfer a pattern to the fused silica surface. The mask pattern is etched into the surface of a fused silica substrate using reactive-ion (or other) etching processes.

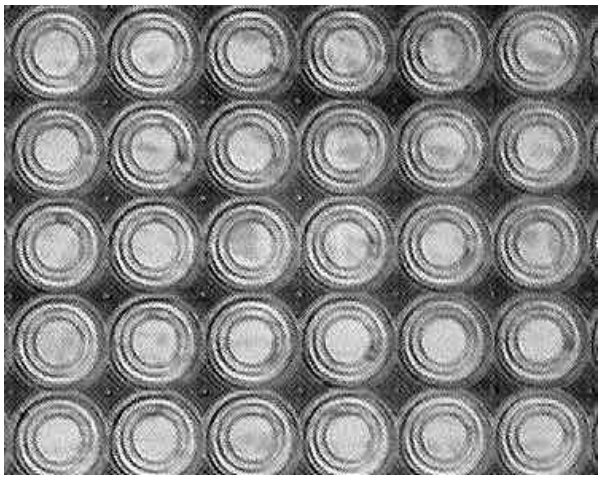

Figure 2 - Detail from a binary optic lenslet array fabricated using micro-photolithography and reactive-ion etching. Each lenslet is 250 mm diameter, and has 16 discrete levels. The lenslets are each f/100.

Since the resulting surface shape of these elements is completely arbitrary, a wide variety of lenslet arrays and other optical elements can be fabricated[7]. These elements

can be made with highly accurate 1 μm features, and RMS surface quality better than λ/20. Figure 2 shows a photomicrograph of a portion of a 74 x 52 lenslet array with 250 μm diameter lenslets.

Another advantage of the wavefront sensor system is its simplicity and robustness. The sensor head consists of only two parts; a lenslet array and a detector array. This combination can be made extremely rigid, and is capable of managing significant vibration and rough handling. For a field system, this is a key requirement.

The total dynamic range is another important attribute. A one-dimensional wavefront sensor used at Sandia Laboratories has been shown to have a dynamic range of 10^4 (the ratio between the smallest detectable change in wavefront slope to the largest measurable slope). This allows a single sensor to measure a large range of optical aberrations and still have high sensitivity. The current generation of WaveFront Sciences sensors have 5-15 μrad noise levels and can measure up to 15 mr. With a different lenslet array, the noise level and range can be adjusted to be 50 μrad and 500 mr.

We have applied the Shack-Hartmann sensor to turbulent flow[8], nuclear-reactor induced flow[9], droplet evaporation[3], and tomographic measurements in a heated jet[4,14]. We are currently using the sensor to measure aero-optic heating effects in hypersonic interceptor seeker windows[10].

1.3 Measurement of aero-optic phenomena

The wavefront sensor measures the phase of incoming light. To measure some aerodynamic parameter, light must be appropriately processed through the fluid. As light with a planar wavefront passes through a fluid, density and/or temperature variations will influence the total optical path, and the phase (or wavefront) of the beam (see Figure 3). These variations in optical path difference can be directly measured and used to infer quantities in the flow.

In order to make measurements in a fluid, there are several key elements to consider:

1.3.1 Integrated line-of-sight

The wavefront sensor inherently measures all of the light incident upon it. This means that the measurement includes an integrated line-of-sight for all elements and aero-phenomena in the optical train. In complex 3D flows it can be difficult to separate effects from various regions in the flow. There are three basic ways to deal with this problem: use the sensor to measure primarily 2D flows, reconstruct 3D data from a series of 2D views (tomography), or use stored reference information to subtract constant or uninteresting flow features.

1.3.2 Optical signal probe

The light must pass through the aero-optical effect in such a way as to pick up the appropriate information. Usually,

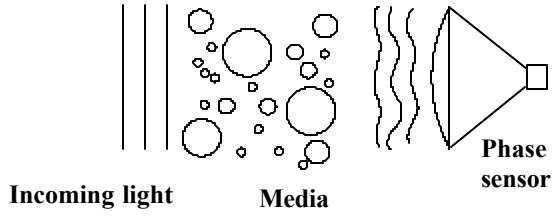

Figure 3 – The phase of light can be a sensitive measure of density or other aero-optic phenomena.

variations in density lead to variations in total optical path length. The wavefront sensor can readily measure these variations. In some cases, it is difficult to introduce the probe beam without perturbing the flow itself. For example, seeker windows may look directly into the flow. A probe measurement is difficult in this case since the use of a mirror or other optical element directly upstream will perturb the flow. Previous papers have addressed this issue, and proposed a method for dealing with it[10].

In other cases, it may be that it is difficult to introduce the optical signal without distorting it. This is true for many of the aero-window effects. In a supersonic wind tunnel, either the light must be introduced through a "baffle plate," which has a window in the supersonic flow, or through a shear layer. In either case, it may be that the light is distorted while introducing it to the flow. The ability to subtract a reference beam may enable some of these applications.

1.3.3 Reference conditions

One key parameter in any optical measurement in fluid mechanics is the definition of exactly what is to be measured. It is extremely difficult to build an optical system with perfect performance, especially when installed near a large wind tunnel or other apparatus. Thus an important ingredient in the measurement process is the ability to establish reference conditions where errors in the optical system may be subtracted from the final measurement. This type of de-referencing, or background subtraction, is commonly applied as a data analysis technique.

The Shack-Hartmann wavefront sensor is ideally suited for reference subtraction in flow systems. The user simply records the focal spot position prior to turning on the flow,

and subtracts these positions from the subsequent data. This serves to subtract the effect of optical system aberrations and to allow the user to concentrate on only the measurements of interest.

1.4 Previous work

1.4.1 Turbulence measurement in temperature gradient flows

At Sandia, a one-dimensional wavefront sensor was used to measure turbulence in flows with large temperature gradients. The temperature gradient served as a thermal marker on the turbulent elements, allowing the wavefront sensor to detect their effects. As flow passed through the region with the temperature gradient, turbulence would have the effect of mixing the hot and cold regions. In these low speed, constant pressure flows, the temperature changes resulted in changes in local density, which was observable by the wavefront sensor through its effect on the local index of refraction. A one-dimensional wavefront sensor that operated at 2.5 kHz was used to make a series of measurements of these flows, and the power spectral density and other important phenomena were derived. The sensor was found to have excellent dynamic range, and exceptional sensitivity. In one experiment, the cyclic heating of fluid elements was observed that had only 0.3 C temperature changes.

1.4.2 Eight view tomography system for heated plume measurements

McMackin et al[4,14] built an eight-view tomography system to separate out the line-of-sight issues. They used eight 1D-wavefront sensors similar to the ones developed in the Sandia efforts3. The system was set up to simultaneously record the views from the various sensors and they were arranged to interrogate a heated free jet flow from all directions. Using this information, a slice through the flow was reconstructed that allowed a point by point measurement. The nozzle height could be adjusted to allow characterization of the entire plume. Several interesting studies were conducted using both forced and unforced oscillations at several Reynold's numbers. The resolution was less than a millimeter for the typically one-inch diameter free jet flows.

1.5 Seeker window aberration measurement

The main goal of the current work is to develop methods for making accurate measurements of interceptor missile seeker window aberrations in high Mach number flows. These measurements are important for next generation interceptors such as the Theatre High Altitude Air Defense (THAAD) missile, the Navy Standard Missile, and other systems employing optical terminal guidance. These systems suffer from the potential image degradation caused by aero-optical phenomena.

There are two primary cases to consider:

- Uncooled, sapphire (or other material) windows that are distorted as a result of aerothermodynamic heating effects. In this case the aberrations are fairly slow to develop (4–5 seconds), but can be strong. In the worst case, the window may fail under the test load. The aberrations are relatively low order; primarily bore-sight error, focus and astigmatism.
- Cooled windows, where the cooling system may introduce significant image aberrations through turbulence. In this case the aberrations may be much smaller, but they are of high spatial and temporal frequency.

Both of these situations must be considered in a seeker window test program, and diagnostics must be developed for each case. The wavefront sensor diagnostics, along with other diagnostics, allow both of these different cases to be measured, although perhaps with different lenslet arrays, light sources or cameras.

The body of this paper describes test methodologies that have been developed for these seeker window measurements, and present some results from laser-spark guide star wind tunnel measurements. Some preliminary work has been completed, and the development of a detailed diagnostic set is in progress.

2. SHACK-HARTMANN WAVEFRONT SENSORS

Shack-Hartmann sensors are sensitive, sophisticated optical measurement devices based on arrays of small lenses, or lenslet arrays, that use CCD cameras as detectors. These wavefront sensors have been successfully implemented in experiments at Sandia National Laboratories, USAF Phillips Laboratory, and MIT Lincoln Laboratory among others[11]. A wavefront arriving at the sensor is sampled at many locations by the lenslet array, which creates a grid of focal spots on the focal plane of the detector (See Figure 1). The position of each focal spot depends on the average wavefront slope over the subaperture formed by each lenslet. By determining the position of the focal spot using centroiding or matched filtering algorithms, the slope structure of the spatial wavefront is determined. The wavefront is reconstructed by matching the wavefront

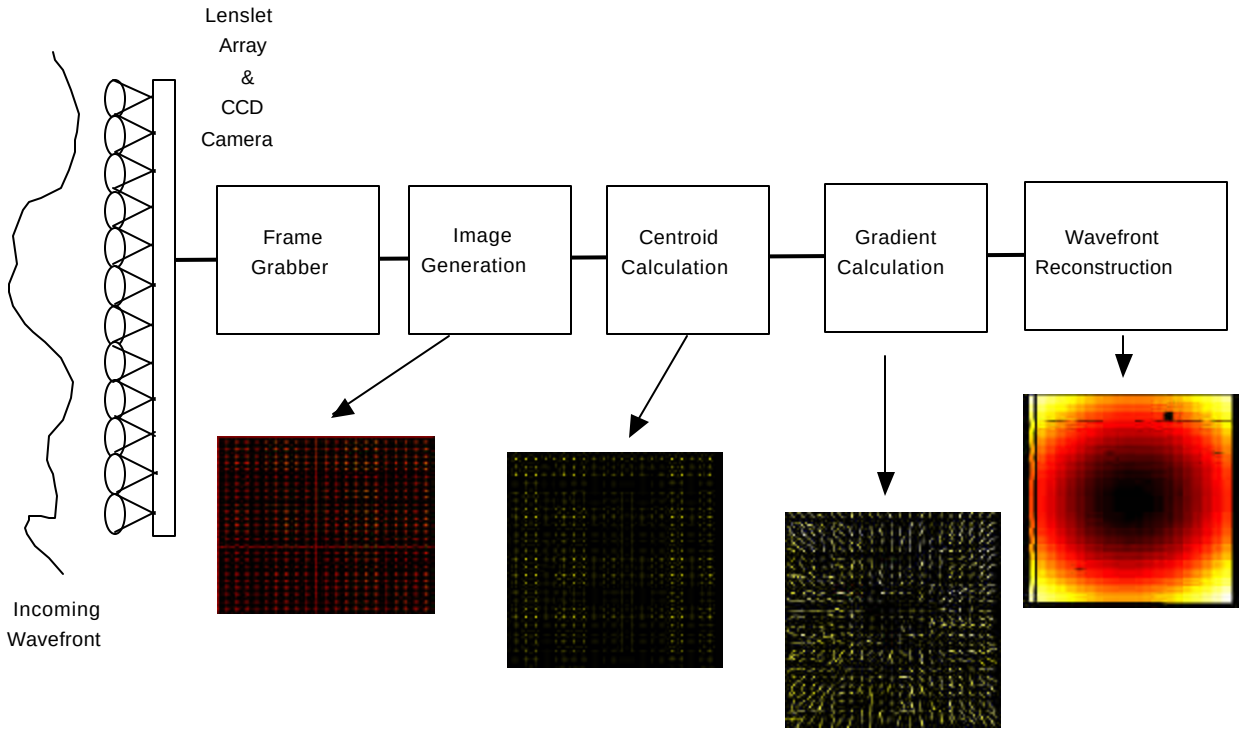

Figure 4 - Basic wavefront sensor operation

height at the edges of adjacent subapertures (each with different slopes) using one of several different wavefront reconstructors.

These sensors have recently become more practical and economical because of advances in optical fabrication technology. Previously, it was very difficult to fabricate an array of small lenses. They either had to be individually ground and polished and then tediously assembled by hand, or made through step and repeat processes with poor fill factor and uniformity. New technologies in the production of optics using binary or diffractive optics technology allow fabrication of extremely complex, yet precise, optics, at a fraction of the cost of other methods. Diffractive optics has advantages over conventional approaches because lenses with diameters measured in tens of μm can be fabricated with high efficiency (>98%) and excellent optical quality. The lenses can be designed to have arbitrary surface profiles, and can be segmented, providing a much more flexible and economical fabrication.

2.1 Sensor Operation

The basic operation of a wavefront sensor system is depicted in Figure 4. Incident light is collected and propagated to the lenslet array in front of the CCD camera. The lenslet array creates a pattern of focal spots on the CCD. The CCD image is broken into subapertures (called Areas Of Interest) of N x N pixels (corresponding to the region behind each lenslet) in which an intensity centroid is found:

$$\hat{r}_l^x = \frac{\sum_{AOI_l} I_{i,j} x_{i,j}}{\sum_{AOI_l} I_{i,j}}, \text{ and } \hat{r}_l^y = \frac{\sum_{AOI_l} I_{i,j} y_{i,j}}{\sum_{AOI_l} I_{i,j}}. \quad (1)$$

The position of the centroids, as compared to a set of reference positions is the central measurement. By appropriate calibration of the wavefront sensor with a plane wave, precise measurements of the aberrated wavefront slope distribution can be made,

$$q_l^x = \frac{\hat{r}_l^x - \hat{r}_l^x\big|_{REF}}{f}, \text{ and } q_l^y = \frac{\hat{r}_l^y - \hat{r}_l^y\big|_{REF}}{f}, \quad (2)$$

where f is the lenslet focal length, q_l^x and q_l^y are the wavefront slopes, and $\hat{r}_l^x$ .and $\hat{r}_l^y$ are the centroid locations. The specific AOI is indicated by the subscript l, and superscript x and y indicate the Cartesian axes.

The processing computer uses the positions of the focal spots on the individual subapertures to generate phase gradients (see Figure 4) from Equation (2). The wavefront is defined as the surface normal to the direction of propagation, so these measured values can be used to

reconstruct the wavefront by numerically solving the gradient equation:

$$\nabla f_l = \left.\frac{\partial f}{\partial x}\right|_l \mathbf{i} + \left.\frac{\partial f}{\partial y}\right|_l \mathbf{j} = q_l^x \mathbf{i} + q_l^y \mathbf{j} \qquad (3)$$

This equation can be solved using a number of modal and zonal methods[12]. The solution is a complete description of the phase distribution for the measured light[13]. The intensity distribution is the total energy measured in each subaperture. This quantity is also easily determined from the measurement.

2.2 Point spread function measurements

As light passes through an optical system under test, the net effect of optical aberrations is degradation in overall image quality. Since it is the image of a target that is important in a seeker system, a direct measure of image degradation is a useful diagnostic of the performance of the system[1]. The point spread function is defined as the response of an optical system to an ideal point source. Conversely, it is the response of an optical system to a purely flat wavefront (point source at infinity). Thus it measures the quality of focus for a real optical system, or the image degradation. A perfect optical system will be limited only by diffraction, and thus have an Airy pattern as the ideal point spread function. For a real optical system, this is somewhat degraded. From Fourier optics, this is the same quantity as the far-field diffraction pattern, except measured in angular space. Thus the terms "point spread function" and "far-field pattern" are used somewhat interchangeably throughout the rest of this paper.

Since the point spread function measures how well the light can be focused, and this is what is measured in an imaging system, it is important to be able to accurately calculate the point spread function from wavefront sensor measurements. If this procedure can be proven to be accurate and reliable, it will be possible to make near field wavefront and intensity measurements, and predict far-field performance. Scaling to different wavelengths, aperture sizes and aberration strength are also possible. Furthermore, the wavefront sensor can be used to make flow on/flow off measurements to subtract out the effect of aberrations in the optical system used to test the window in the wind tunnel. Thus the important effects (window aberration or turbulence) can be isolated from other optical issues.

The point-spread function (for a source at infinity) can be measured directly with a lens placed one focal length away from a detector. This type of measurement can be made in the wind tunnel as well. In fact, this has been applied in a number of different tests at various wind tunnels [1].

There are several advantages to this technique. It is conceptually simple, and needs little interpretation. A direct measurement of the Strehl ratio can be obtained by comparing flow on/flow off results. This number can be used directly in system modeling and other performance indexes.

However, there are also some drawbacks. The point spread function measurement is inherently absolute. It gives information only about the total wavefront received by the final imaging lens. Aberrations introduced by the upstream optical system (whether or not they were caused by aero-optic effects) will lead to degradations in Strehl. This means that, either the optical system used to direct the light into and out-of the wind tunnel must be extremely high quality (< $\lambda/10$ overall), or only relative measures of Strehl can be obtained. Unfortunately, Strehl ratio is not linear with respect to RMS wavefront error. If the optical system is not perfect, it is difficult to separate the aero-optical effects from the optical system effects.

While the point-spread function has more information than just the Strehl ratio, it is difficult to interpret. The point spread function $P(f)$ can be written:

$$P(f) = \left|F\{U(x,y)\}\right|^2 \qquad (4)$$

where $F\{\}$ represents the complex Fourier transform, and $U(x,y)$ is the complex field of the light incident upon the final imaging lens. This quantity is purely real, and contains no phase information. The Strehl ratio is defined as:

$$S = \frac{P_{\max}}{P_{\max}^{Ideal}} \qquad (5)$$

where $P_{\max}$ is the maximum value of the point spread function of the optical system including the optical errors, and $P_{\max}^{Ideal}$ is the maximum value of the point spread function for a system without errors. This number does not contain any information about the structure of the errors. Since the mathematically equivalent operation of a lens is the Fourier transform, light will be scattered out of the central

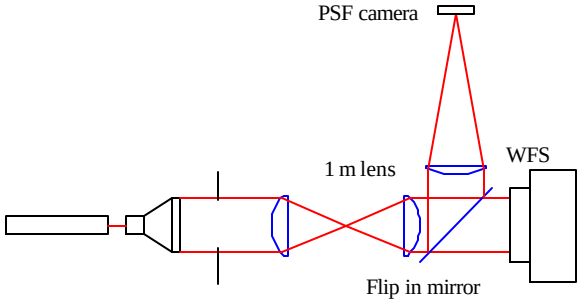

Figure 5 – Setup for comparing WFS derived point spread functions to a direct measurement.

lobe in a direction depending upon the spatial frequency (*f*) of the incident wavefront. Therefore, additional information can be obtained related to the scattering angle. In fact, the PSF can be interpreted as the power spectral density of scattered light with respect to angle.

The drawback of the PSF is that it cannot be inverted by simple means. The phase information is lost when the intensity distribution is obtained (i.e., when the magnitude-squared of the field is computed). Therefore, while it is possible to obtain some useful information about the overall effect of the optical errors, it is not possible to determine their source or cause. Many different wavefront distributions can result in the same (or similar) PSFs. One cannot simply subtract one point-spread function from another to determine the effect of changes in the optical system because the phase information has been lost in measuring the PSF.

The Shack-Hartmann wavefront sensor measures both aspects of light: irradiance and phase distributions. Given this information in the near field (i.e., incident upon the final imaging lens), the PSF can be computed. The far-field amplitude is given by (where *u* and *v* are the far-field angles):

$$U(u,v) = \int_{-\frac{a}{2}}^{\frac{a}{2}} \int_{-\frac{b}{2}}^{\frac{b}{2}} U(x,y) \exp\left[-\frac{2p}{l} i(xu + \right.$$

where *U(x,y)* is the near field complex field given by:

$$U(x,y) = \sqrt{I(x,y)} e^{\frac{2pi}{l} f(x,y)},$$

and *I(x,y) is* the measured irradience distribution and *f(x,y)* the wavefront height distribution. Note that Equation 6 represents the Fourier transform of the input field *U(x,y)* with respect to *u* and *v,* hence Equation 4, 6 and 7 can be used together to compute the PSF from the wavefront and irradience distributions.

Measuring the near field irradiance and wavefront distributions, and then computing the PSF, has a number of advantages over direct PSF measurement:

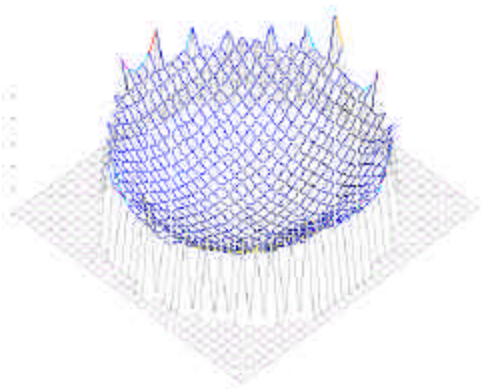

Figure 6 – Wavefront error for defocus laser beam test. This is a 0.55 mm peak to valley and .084 mm RMS.

- The wavefront sensor's relative mode operation can be used to estimate effects induced by the flow, rather than that of the total optical system.
- The flow-induced aberrations can be directly determined by examining the wavefront.
- The image size and structure can be determined at an arbitrary plane in the optical system by Fresnel

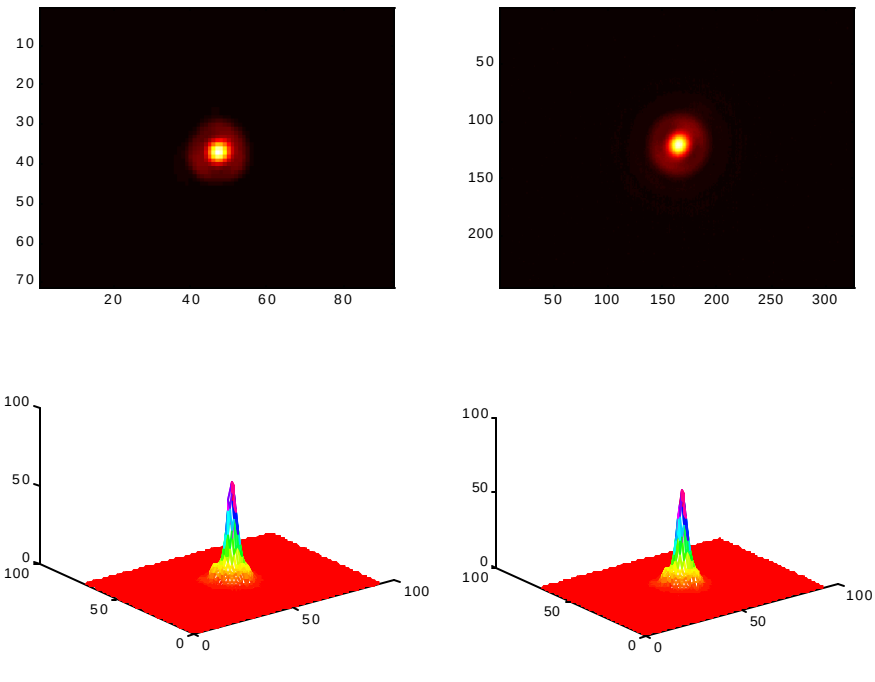

(a) (b)

Figure 7 – Point spread function for a 7.8 m radius of curvature input wave. (a) Computed from wavefront sensor data. (b) Measured by the PSF camera.

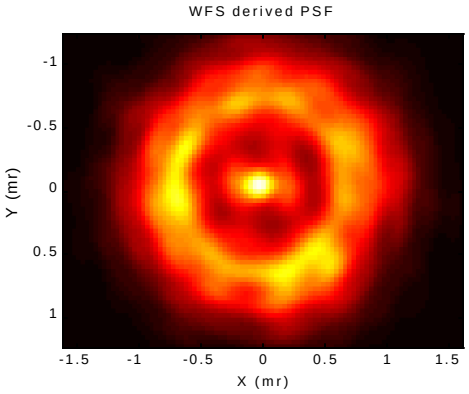

(a)

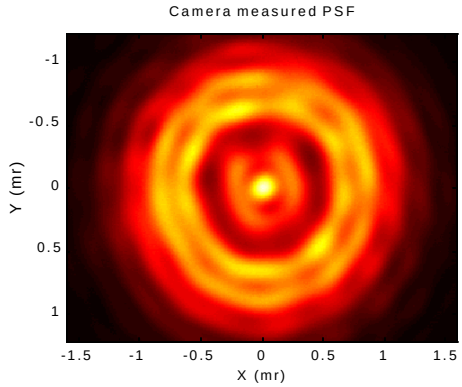

(b)

Figure 8 – Comparison of (a) WFS derived PSF and (b) imaging camera measured PSF for strong defocus. The peak-to-valley wavefront error was 1.3 mm and the RMS WFE was 0.29 mm.

propagation analysis.

- Zernike and other aberration coefficients can be determined to allow characterization in terms of common optical system errors.

To determine the feasibility of this measurement technique, a simple laboratory experiment was conceived and set up as shown in Figure 5. In this case a 1:1 imaging telescope was set up with two 260-mm focal length achromats. These were arranged to image an iris onto the lenslet array of the wavefront sensor or, alternatively (if the flip in mirror was in place), onto the imaging lens. This allows data to be acquired with both the wavefront sensor and PSF camera in rapid succession. Various aberrations were then introduced into the beam and the results recorded from each instrument.

The simplest aberration to induce is a defocus error. (Actually tilt is simpler, but it only affects the PSF by moving the center point, and thus is of no interest to these calculations.) By moving the position of the second lens by a small (or large) amount, a varying amount of defocus can

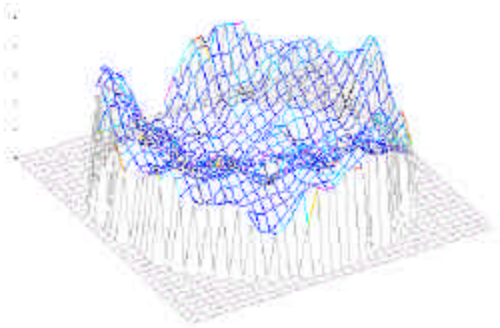

Figure 9 – Wavefront error for turbulence simulator. The total RMS wavefront error was 0.18 mm and the peak to valley wavefront error was 0.92 mm.

be introduced to the optical train. This will result in a spherical wavefront measured by the wavefront sensor (see Figure 6), and a defocused spot by the PSF camera. Results

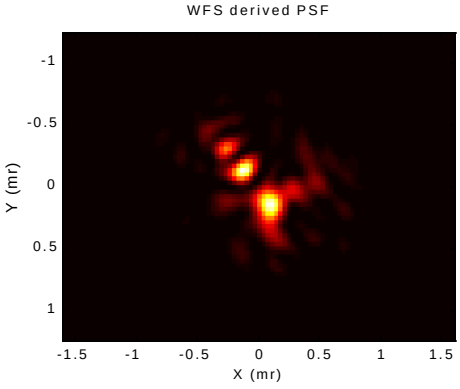

(a)

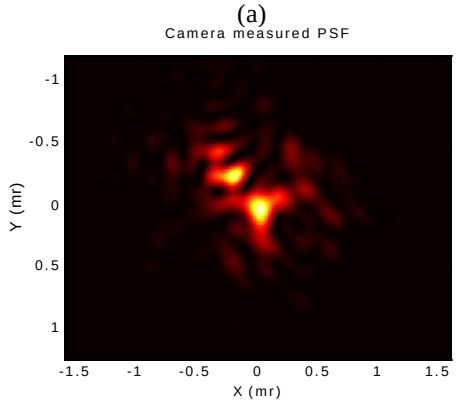

(b)

Figure 10 – (a) Wavefront sensor predicted and (b) imaging camera measured point spread function from large scale turbulence (0.29 mm RMS WFE)

from this measurement are presented in Figure 7 and Figure 6. The wavefront sensor was used to measure the phase and intensity at 0.633 nm, and equations 4–7 were used to predict the point spread function. In this case, the defocus was not very large (7.8 m radius of curvature), and so the point spread function has a strong central peak, surrounded by a "halo." This is very typical for low order aberrations that are fairly small (λ/7.5). For a large defocus case, as shown in Figure 8, the central lobe has very little residual energy, and the halo dominates the PSF. Here the total wavefront error was 2.1 waves peak to valley and 0.45 waves RMS. Nearly all of the light is diffracted.

The important point of both of these figures is that, for low order aberrations, the wavefront sensor accurately measures the wavefront and predicts the point spread function. Window aberrations for an uncooled supersonic interceptor seeker window are expected to be low order tilt, focus and astigmatism. For this case, we expect that wavefront sensor measurements should lead to accurate predictions of the seeker image.

However, these low order aberrations are vastly different from those imposed by turbulence. Turbulence can be a combination of both high spatial frequency and high RMS wavefront error. This combination leads to very high scattering angles, and can lead to a significantly degraded PSF. In future work, wavefront sensor measurements are planned to evaluate turbulence measurements in the supersonic wind tunnel. Prior to these expensive tests, a laboratory evaluation of the response of the wavefront sensor to these higher order effects is needed. To this end, a simulation of the turbulence environment is necessary.

There are several ways to simulate turbulence. Neal et al used a small wind tunnel with a strong temperature gradient to create grid turbulence from a wire mesh[8]. They used a wavefront sensor to characterize the turbulence as it propagated downstream. McMackin et al[14], used a heated free jet to create turbulence. However, both of these experiments involved expensive, although small scale, wind tunnels, so that the turbulence could be controlled and characterized. For testing of the wavefront sensor accuracy, these are extraordinarily expensive methods. Thus another method was sought.

Micro-optics technology has been used to make a wide variety of optical elements. The surface of the optic can be described point by point from numerical data and accurately produced in practice. This technology is the same technology used to make the lenslet arrays used for the Shack-Hartmann sensors. Using numerical simulation, a phase screen was developed to describe the phase delay introduced by propagation through turbulence. The simulation allowed for several different look angles and turbulence strengths. This phase screen data was used to

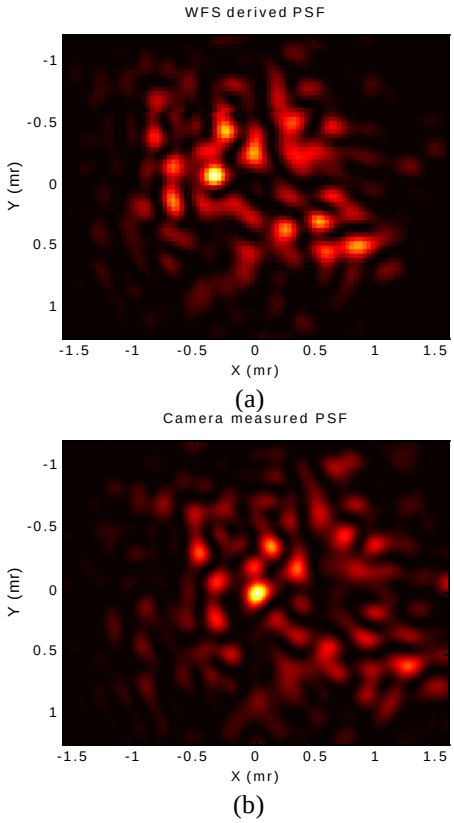

Figure 11 – (a) Wavefront sensor computed PSF and (b) measured PSF for simulated atmospheric turbulence with small structure size and moderate strength. The RMS wavefront error was 0.28 mm and the P-V was 1.8 mm.

construct a micro-optic to impose the appropriate phase structure on light passing through it. This element was used in the laboratory setup to test the wavefront sensor response to turbulence. The micro-optic had five different zones, with different scale sizes in each. In addition, the simulated turbulence strength varied from one end to the other.

This atmospheric aberration simulation element was used to test the effects of turbulence on the wavefront PSF prediction process. The optic was placed at the location of the iris in Figure 5, and relay imaged onto the WFS lenslet array or PSF camera lens. The results are shown in Figure 9 and Figure 10. The wavefront sensor predictions show excellent agreement with the measured PSF. While there are some small discrepancies for the intensity distribution, the overall pattern is replicated extremely well. The small discrepancies may be due to difficulty in finding the exact location of the focal point of the imaging lens. A 1-m focal length lens has a considerable depth of field, so this point is hard to locate. It was observed that the detailed energy distribution was somewhat sensitive to this location.

For turbulence with the same strength (i.e., the same RMS wavefront error), but smaller structure size, the light scatters

into a much larger speckle pattern. This can be seen in Figure 11 for both the WFS computed PSF and the measured PSF. Even in this case of extremely small structure size, the wavefront sensor is able to make accurate predictions.

3. SUPERSONIC WIND TUNNEL EXPERIMENTS

A series of wind tunnel experiments has been planned for a program lasting several years. The early experiments are aimed at establishing the facility effects and developing the diagnostics, with later runs aimed at validating the test concept with windows in simulated models. Both turbulence and window distortion effects will eventually be evaluated, with full-scale interceptor nose-cone models being used in the final tests. We have completed some preliminary experiments at Mach 8, and have begun the facility effects experiments at Mach 7. In addition, we have completed an initial spark source experiment at Mach 8. Some of the facility effects results will be reported, and a description of the laser-spark guide star. Further results will be released as the program develops.

3.1 Wind tunnel facilities

The primary wind tunnel facilities used for this program are the Tunnel 9 hypersonic tunnels at White Oak, MD. Figure 10 shows one of the three tunnel legs configured for Mach 8 operation. These facilities are capable of 4 second run times at Mach 7 and 0.7 seconds at Mach 8. With these long run-times, there is time for significant heat transfer to take place. This will create a realistic simulation of the aero-thermal effects in model seeker windows. The wind tunnels can be configured for a variety of flow regimes and Mach numbers, and can run approximately once a day.

3.2 Diagnostics

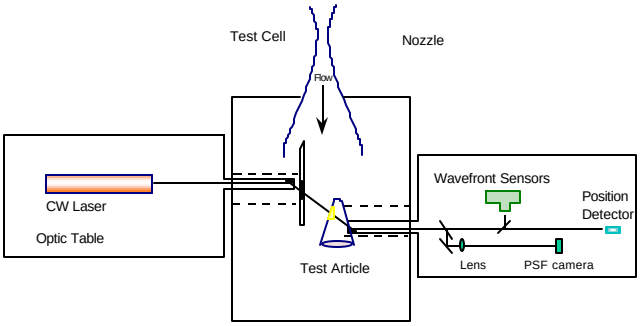

Figure 13 – Test setup for window aberration measurements. The light is introduced through a baffle plate that is placed in the Mach 7 or 8 flow.

Figure 13 shows the diagnostics table layout for the initial wind tunnel experiments. These consist of two different

Figure 12 – AEDC White Oak Tunnel 9 facilities. The wind tunnel can be configured for a variety of different flow conditions and Mach numbers.

wavefront sensors, a tip/tilt quad cell sensor, and a direct PSF camera, along with the appropriate optical elements to direct the beam onto the appropriate sensor. All the diagnostics are fed through a single probe beam directed through the window or appropriate path. This beam has been expanded to approximately 1-inch diameter, and a 5:1 telescope (not shown) is used on the diagnostics table to reduce the beam footprint to match that of the various sensors. This telescope is also set up to re-image approximately the center of the wind tunnel. This helps to make sure all of the light is collected by the diagnostics system and is not lost through clipping on downstream optics. It also provides for a common object plane against which all sensors can be referenced.

3.2.1 Wavefront sensors

Two different custom wavefront sensors are used for the flow diagnostics. They are direct derivatives of the CLAS-2D wavefront sensor produced by WaveFront Sciences, Inc.. These sensors incorporate the lenslet array, camera, data acquisition electronics, computer and analysis software into a single unit. This allows for rapid data acquisition and control, and provides for acquisition of several hundred frames of data at high rates. The data may be processed in a variety of ways and the results exported to various formats for comparison with other sensors. Two different sensors were configured for these experiments:

- Pulnix 6701 camera with 8-mm focal length lenslet array. This sensor has 0.144 μm resolution and can run at up to 120 Hz. Full frame mode (normal) is 60 Hz. The camera can be asynchronously reset for use with pulsed lasers.
- Pulnix 9701 camera with 25-mm focal length lenslet array. This sensor has 0.252 μm resolution and runs at 30 Hz.

This camera has full asynchronous reset capability and has an eight bit digital output bus.

Both of these wavefront sensors were precalibrated to precisely place the lenslet array one focal length in front of the detector. In addition, a plane wave reference file was recorded to facilitate absolute measurements. Either system can be used in either absolute (use the plane wave reference) or relative (use recorded images from just before the wind tunnel run) mode.

The CLAS-2D analysis and control software has all of the centroid, wavefront slope and wavefront reconstruction functions built in. In addition, it allows for numerous graphical displays, and can perform Zernike decomposition and far-field PSF calculations.

3.2.2 Quad cell measurements

Since facility and other vibrations are likely to be a dominant source of time-dependent misalignment, a high bandwidth, position sensitive detector was used to monitor these effects. The system consisted of a long focal length lens (1 m) and a UDT position sensitive detector. This detector can operate at up to 3 kHz and detect simultaneous tip and tilt motion. While it only monitored the single, lowest order, aberration component, the increased bandwidth allowed determination of aliasing effects on other sensors.

3.3 Wind tunnel runs

3.3.1 Facility vibration effects

Facility induced vibration is one of the key technical issues to be overcome in order to make accurate window aberration measurements. To assess this vibration, a number of simple experiments were devised. These consisted of the following approaches:

- **Simulated optical system**. The sensor system was set up with optical tables in place next to the wind tunnel, with a cw probe beam instead of the laser spark. This allowed monitoring of the vibration at higher bandwidth than that limited by the repetition rate of the YAG laser. The beam was directed over the top of the tunnel, without actually interacting with the flow at all. Using this arrangement, it was determined that acoustic noise was strongly coupling into the optical system. Measured noise levels were around 130–140 dB. To reduce this coupling, the optical tables were mounted on vibration isolation platforms and completely enclosed in anechoic foam lined boxes. This reduced the noise level to ~100–110 dB from 120-130 dB.

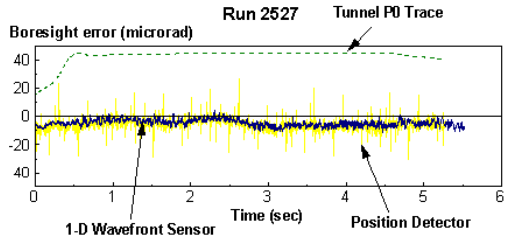

Figure 14 - Mach 7 wind tunnel results for recirculation zone experiments. The total error was less than ±10 mr.

- **Recirculation zone probe**. The wind tunnel test section is five foot in diameter, with an 18-inch diameter hypersonic nozzle. This means that there is a large recirculation zone that is not directly involved in the hypersonic flow. It is not expected that there should be large temperature or density gradients in this region of the flow. For further vibration testing including the effects of wind tunnel injection and inspection window vibration, the light was sent through this recirculation zone, but not through the hypersonic flow region. In this case the measured vibration resulted in less than ±10 μr of tilt, as seen in Figure 14. This is a very encouraging result, indicating that it is possible to make high fidelity measurements through the wind tunnel, in spite of the huge amount of acoustic noise and other induced vibration. Recent results with an improved diagnostics set have confirmed these results.

3.3.2 Window aberrations at Mach 8.

At Mach 8, the window heating effects are much reduced due to an initially cooler overall flow, shorter run time (0.7 seconds). The Mach 8 condition is thus much less stressing on the optical components than the Mach 7. Baffle plates and other optics may be used directly in the flow. An initial set of experiments was conducted at this condition to evaluate various facility effects, and to test end-to-end wavefront sensor data acquisition and analysis. These results, while promising, were compromised due the presence of fringes in the optical beam from the thick windows in the test section. These fringes were initially thought to be unimportant, but have proved difficult to remove in data analysis. To avoid fringes, two approaches have been developed: (1) use AR coated windows with sufficient wedge that the reflections from each surface do not overlap, and (2) use a broad band source to reduce the fringe contrast in overlapped regions. Of these, item (2) has been explored at some depth. A fiber-coupled diode laser source has been developed with a multi-mode diode. By carefully adjusting the current and junction temperature, this

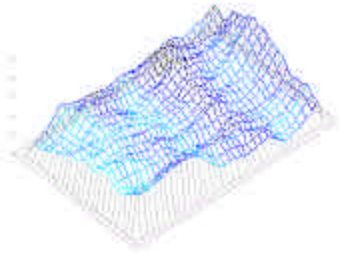

(a)

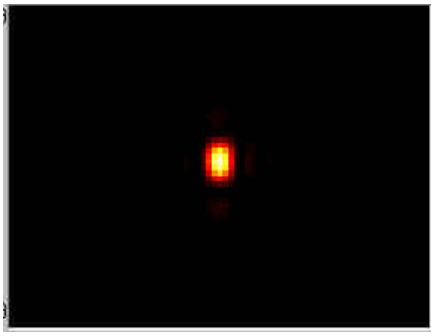

(b)

Figure 15 – Mach 8 wind tunnel results for early in the run (0.1 second) (a) wavefront error and (b) point spread function. The RMS wavefront error was 0.022 mm, P-V wavefront error was 0.14 mm and the Strehl ratio was 0.95.

source runs in several modes for an extended period of time. In addition, the vibration environment at Mach 8 was found to be significantly worse than that at Mach 7. Vibrations in the +/- 40–50 μr were frequently observed. Since the run time was short (0.7 sec), and the 2D wavefront sensor data acquisition rate was 30 Hz, relatively little data was obtained (approximately 40 frames). Nevertheless, it was possible to observe significant degradation in the optical quality of the window.

Figure 15 shows the wavefront error and point spread function from early in the wind tunnel run. This frame occurred before the supersonic flow had reached the steady state Mach 8 condition. In this case there is some residual RMS wavefront error (0.22 μm) from turbulence and other flow effects, but the overall image quality is quite good (0.95 Strehl ratio). However, as the run progressed, the window was continually heated. Figure 16 shows the wavefront error and point spread function at 1.2 seconds into the run. For this case, steady state conditions at Mach 8 last for about 0.7 seconds, but supersonic flow continues until about 1.5 seconds. The wavefront error has increased dramatically

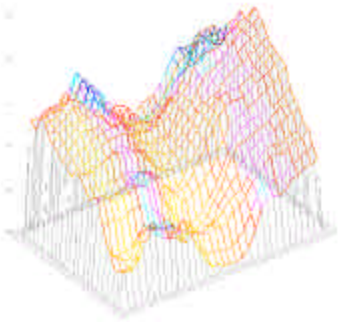

(a)

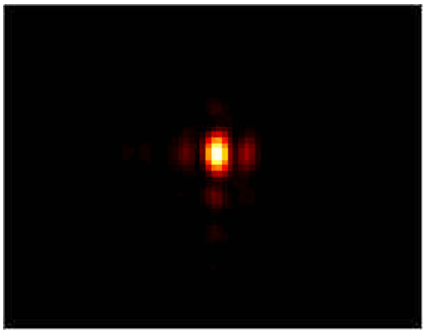

(b)

Figure 16 – Mach 8 wind tunnel results for late in the run (1.2 seconds). (a) wavefront error and (b) point spread function. The RMS wavefront error was 0.078 mm, and the P-V wavefront error was 0.40 mm. The Strehl ratio was 0.55.

(~factor of 3) which leads to a significant degradation in the overall image quality. The Strehl ratio has been reduced to 0.55, with the light diffracted into higher order lobes. While these images are still not to bad, in terms of overall appearance, the window in this case was only measured over a 8.8 X 6.5 mm region. The total seeker window in this case was much larger (roughly 40 X 80 mm). The window was mounted in a wedge plate assemble that held it at 5° to the flow. Furthermore, the 0.7 seconds of heating is much lower than that expected for realistic flight conditions.

At Mach 7 all of these conditions become much more stressing. The run time is much longer, resulting in more time for heat transfer to take place. Also the static temperature is much higher at Mach 7. Since the total window aberrations are of interest, a large portion of the aperture will be monitored (using a 5:1 demagnification system), and thus more total aberration will be measured. Further more, note that 5° is not a large angle of attack. Realistic missile forebodies are more like 20-30° angle of attack. In total, much stronger aberrations are expected at the realistic flight conditions. Yet the wavefront sensor was

able to make measurements for these cases with minimal aberrations and get good measurements in the presence of vibration and other noise effects.

One of the key advantages of the wavefront sensor measurement system is evident in the comparison of Figure 15 and Figure 16. When the flow sequence is started, there is a short time before flow really begins. During this time, the test cell is essentially at vacuum conditions. For the analysis shown in Figure 15 and Figure 16, the first frame of data was used as a reference condition. Thus any errors in the optical system or static aberrations in the windows were completely subtracted out. These figures represent the flow induced effects only, and the PSF plots the result of window heating on the image quality. With other methods it would be very difficult to separate the effect of window heating from optical system or other errors.

3.4 Future work

Significant future work is planned to further characterize facility vibration and other effects, to develop better light sources, and to perform experiments in the wind tunnel for both wavefront sensor and PSF camera instruments. In addition, turbulence measurements using a pulsed laser will be performed along with a variety of other experiments.

4. CONCLUSIONS

We have applied the Shack-Hartmann wavefront sensor to the measurement of hypersonic missile interceptor seeker windows. We demonstrated that the prediction of the point spread function from near field wavefront sensor measurements gave accurate results using a laboratory mock up and simulated aberrations. We applied the wavefront sensor to flow measurement at Mach 8, and have begun to develop the appropriate hardware for Mach 7.

The wavefront sensor gives an extremely robust way to measure window aberration, turbulence and other phenomena with good accuracy. The image degradation can be readily calculated from the measurements, and a variety of useful quantities can be inferred. Since a reference wavefront can be easily subtracted from the measurement, errors in the optical system can be subtracted out from the measurements. This allows a true comparison of flow on/flow off behavior.

ACKNOWLEDGMENTS

This work was supported by Sandia National Laboratories and the Naval Surface Warfare Center Work For Others contract number 011960104A and Sandia contract number AV-0910.

REFERENCES

[1] M. S. Holder, R. A. Parker, B. J. Walker, "Interceptor testing in the LENS aerothermal/aero-optical test facility," Paper No. 10-02, 6th AIAA/BMDO Technology Readiness Conference, August 18-22, 1997, San Diego CA.

[2] R. A. Willett, J. Xerikos, J. J. Grossman, "Hypersonic wind tunnel measurements of optical signal distortion due to propagation through cooled-window mixing layers," SPIE Vol. 2005, pp.103–115 (1993).

[3] D. R. Neal, T. J. O'Hern, J. R. Torczynski, M. E. Warren, and R. Shul, "Wavefront sensors for optical diagnostics in fluid mechanics: application to heated flow, turbulence and droplet evaporation," SPIE Vol. **2005**, pp. 194–203 (1993).

[4] D. Neal, R. Pierson, E. Chen, K. Bishop, and L. McMackin, "One dimensional wavefront sensor development for tomographic flow measurements," SPIE vol. **2546**, pp. 378-390 (1995).

[5] See for example, SPIE Vols. **1542**, **1920** and **2201**

[6] See for example SPIE Vols. **1544**, **1992**, **CR49**, and **2152** for many papers on binary and diffractive optics.

[7] D. R. Neal, J. D. Mansell, J. K. Gruetzner, R. Morgan, M. E. Warren, "Specialized wavefront sensors for adaptive optics," SPIE Vol. **2534**, pp. 338348 (1995).

[8] T. J. O'Hern, R. N. Shagam, D. R. Neal, A. J. Suo-Anttila, and J. R. Torczynski, "Downstream evolution of turbulence from heated screens: Experimental and analytical results," Sandia Report SAND92–0480 (1992).

[9] J. R. Torczynski and D. R. Neal, "Transient gas motion in nuclear reactor-pumped lasers: computational and experimental results," Nuclear Science and Engineering **113**, 189–206 (1993).

[10] D. R. Neal, D. J. Armstrong, E. Hedlund, M. Lederer, A. Collier, C. Spring, J. Gruetzner, G. Hebner and J. Mansell, "Wavefront sensor testing in hypersonic flows using a laser-spark guide star," SPIE Vol. **3172**-36 (1997).

[11] R. Q. Fugate, "Observations of faint objects with laser beacon adaptive optics," SPIE Vol. **2201**, pp. 10–21 (1994).

[12] W. H. Southwell, "Wave-front estimation from wave-front slope measurements," J. Opt. Soc. Am., Vol. **70**, No. 8 (August 1980).

[13] D. R. Neal, W. J. Alford, and J. K. Gruetzner, "Amplitude and phase beam characterization using a two-dimensional wavefront sensor," SPIE Vol. **2870**, pp. 72–82 (1996).

[14] L. McMackin , B. Masson, N. Clark, K. Bishop, R. Pierson, and E. Chen, "Hartmann wave front sensor studies of dynamic organized structure in flowfields," AIAA Journal **33** (11), pp. 2158–2164 (Nov. 1995)